FFEMS Fatigue & Fracture of Engineering Materials & Structures

doi: 10.1111/j.1460-2695.2012.01650.x

New experimental set-up to approach pipeline fracture behaviour by three-point bending specimens

M. MINOTTI and P. SALVINI

Department of Mechanical Engineering, University of Rome "Tor Vergata", Via del Politecnico, 1, 00133 Rome, Italy

Received in final form 23 October 2011

ABSTRACT A new experimental set-up for drop weight tear tests is proposed. Its principal characteristic is the adoption of inclined supports driving the hinges connected to the specimen. This choice accomplishes the need that the specimen was subjected to a persistent stress field in the ligament, thus approaching the stress field experienced by a crack propagating in a pipeline. This set-up requires a proper processing of the data that is accurately explained in the paper. The tests are conducted under a quasi-static loading but the method has been designed to apply in dynamic tests.

Keywords Drop Weight Test; fracture propagation; pipelines.

NOMENCLATURE

a = horizontal offset of the hammer contact point
a' = value of a taken account the specimen stiffness
cut = number of frame in which the two steps are joint
$D^{(R|L)}$ = contact points of rectilinear bar and hinges
$disp$ = vertical displacement of the rectilinear bar
$Drop$ = vertical displacement of the hammer contact point
$\boldsymbol{E}_{EndCon}$ = energy lost in the specimen connections
$\boldsymbol{E}_{Flow}$ = energy associated to longitudinal stretch
$\boldsymbol{E}_{Frict}$ = energy lost in overall frictions
$\boldsymbol{E}_{Lig}$ = energy of the bending at the ligament section
$\boldsymbol{E}_{TOT}$ = total energy put in the system
$F^{(R|L)}$ = intersection between supports and rectilinear bar
$\boldsymbol{F}_{Lig}$ = axial load
$\boldsymbol{F}_{Frict}$ = value of friction force
$\boldsymbol{F}_{Res}$ = residual value of the friction force
$flow$ = horizontal displacement of the specimen
$G^{(R|L)}$ = contact points of the hinges with the supports
H = height of the specimen
$\mathcal{J}^{(R|L)}$ = Centres of bolted connections
L = distance between F^L and F^R points
L_0 = initial length between the axes of the hinges
$L_0{}^{CT}$ = initial length in the second step for *Combined Test*
L_C = distance between contact points on supports
L_f = distance between D^L and D^R points
Lev_{Frict} = arm of the friction force momentum
Lig = actual value of residual ligament
L_S = length of the specimen

Correspondence: Pietro Salvini. E-mail: salvini@uniroma2.it

$M^{(R|L)}$ = mobile markers applied on the specimen
$\boldsymbol{M}_{EndCon}$ = average bending momentum at the connections
$\boldsymbol{M}_{Lig}$ = bending momentum at the centre of specimen
m_{rect} = the slope of the generic rectilinear line
$\boldsymbol{M}_{Res}$ = residual value of the bending moment
$O^{(R|L)}$ = centres of the hinges
of = offset of rectilinear bar
$\boldsymbol{P}$ = value of the hammer load
Q = middle point of the residual ligament
q_{rect} = the *y-intercept* of the generic rectilinear line
r = radius of support hinges
$\boldsymbol{R}^{(R|L)}$ = frictionless reaction loads
$R_{x,y}$ = coordinates of the centroid of the hammer marker
$Shift_{x,y,\theta}$ = values of shifts for *Combined Test* procedure
$T_{x,y}$ = coordinates of the crack tip
W = intersection between the lines of the reaction loads
x_i,y_i = coordinates of the generic point i
α = angle of the inclined supports
γ = horizontal attitude of the rectilinear bar
$\Gamma^{(R|L)}$ = rotation of the specimen halves at the connections
δ = relative rotation of the two specimen halves
δ_{in} = last value of δ in the first step for *Combined Test*
$\Delta_{x,y}{}^{(R|L)}$ = differential coordinates of marker centroids
ϑ = complementary angle of the support slopes
$\theta_0{}^{(R|L)}$ = initial inclinations of the specimen markers
$\theta^{(R|L)}$ = actual inclinations of the specimen markers
λ = inclination of bisector of the halves opening angle

INTRODUCTION

In the last 40 years, a considerable rise in the mechanical characteristics of pipelines has been reached. Both pipeline diameters and operating pressures have increased, with the aim to improve the overall mass flow rate. [1]

New generations of pipelines followed one another, so that ductile steels could reach hoop stress limits even above 600 MPa.[2] In the typical used scale of strength, the evolution began from the X52 API up to the recent X100 or X120. However, up to now, the new installations of pipelines foresee the extensive use of X80 that is considered mature enough to satisfy all safety and economic requirements.

Ductile fracture resistance of pipelines is an important issue to ensure that any possible catastrophic event might be confined to a delimited area. To this goal, a considerable number of full-scale burst tests have been performed all over the world;[3] all test results concern the capability to arrest the running of a longitudinal crack within the tested pipeline.

The key aspect is the correlation between the experimental tests conducted in a laboratory context and the results of full-scale burst tests. Fracture behaviour of pipelines is usually detected by Charpy V-notch (CVN) tests or by dynamic three point bending tests (DWTT). In this paper, the attention is mainly focussed on DWTT that seems more reliable for high-grade steels.

Improving the correlation involves a better effectiveness of the design criteria, necessarily based on laboratory tests.

A first important difference between laboratory tests and pipelines comes out from the nominal stress. The nominal value in a pipeline differs from the nominal stress applied on the DWTT laboratory specimens. A second aspect regards the longitudinal stretching of the pipe in a burst test that demonstrates the presence of a consistent longitudinal loading during crack propagation. As a matter of fact,[4] the profile of the broken pipe presents a consistent number of folds, documenting an increased length of the opening surfaces. Therefore, the pipe experiences, close to crack tip, a two-dimensional stress field while the DWTT laboratory specimens are affected only by bending, which involves a monodimensional stress.

This correlation was well fulfilled if applied to the lower API-grade pipes. The developed models make use of a balancing between the driving and the resistance force,[5] available during a crack growth. The driving forces are given by the work performed by gas pressure on the opening flanks; this energy is linked to the chemical

composition of the gas itself as well as to its thermodynamic conditions. The resistance force is the result of several phenomena such as material ductility, interaction with the soil surrounding the buried pipeline, inertial loads and so on. The method assumes that the two balancing forces are independent each other, except for crack speed. The intersection between the two *drive* and *resistance forces* points out the existence of a ductile stable propagating speed.

The resistance curve is found by means of CVN measurements, which are elected to be representative of the ductile behaviour during fracture propagation. The method is appropriately tuned for low-grade pipelines. However, poorer results are obtained on high-strength pipelines, even if some correcting factors were *a posteriori* introduced.[6]

A different approach has therefore been suggested.[7] It exploits the results given by an instrumented Drop Weight Tear Test. These tests are conducted on a flattened specimen that is taken from the pipe in full thickness. Among all the possible approaches based on the energy measurement during the crack propagation, those formulated on Crack Tip Opening Angle (CTOA) evaluation seem very promising; they are more and more accepted as arrest/propagation indicator for gas pipelines.[8] Their typical framework is the assessment of a stable running condition. Nevertheless, recent results demonstrated their validity in the computation of non-stationary crack propagations, until crack arrest detection.[9] The CTOA approach, with some adjustments through the introduction of the Work of Fracture,[10] is able to manage non-stationary propagation phenomena, such as the crossing of crack stoppers or any longitudinal change in the pipeline geometry or in the burying conditions.[11]

However, in the case of high-grade pipelines, the fracture criterion based on CTOA shows some discrepancies with the burst test results, and some careful considerations should be carried out. As a matter of fact, the fracture mechanism considered could not reflect the real situation experienced by the steel when the fracture grows.

Several specimen geometries, different from SEN-B, have been proposed for a more reliable application of the CTOA criterion. Among them: conventional compact tension specimens C(T) and middle tension specimens M(T),[12] Three-Point Bending specimens 3-PB [13] or multiple constrained specimens – able to include a larger amount of the plastic region ahead the crack tip.[14,15]

In this paper, possible causes of discrepancy are first discussed and then an innovative experimental lay-out is proposed. This lay-out is applied on DWT Tests, so that the fracture mechanism was closer to the one experienced by the pipe while a longitudinal fracture is running.

The method is applied on quasi-static tests performed on an instrumented tensile test device. Image processing of subsequent frames of the test area allows the evaluations of the parameters required. The attention is primarily focussed on the test layout and on experimental data manipulation, in spite to get information concerning crack behaviour. Unlike the classical DWTT layout, here the specimen is forced to slide on sloped supports, whose angles can be appropriately selected.

APPLICATION OF CRITICAL CTOA ON PIPELINES

There are many reasons that make the fracture development in a pipeline different from the fracture advancement in a DWT Test. Average crack speeds are obviously very different; furthermore, the regions where the crack tips develop are interested by non-matching stress and strain fields.

The plastic zone ahead the crack tip in pipelines can generally extend even more than a diameter, especially in the longitudinal direction. The nominal stress filed is remarkably two-dimensional in pipelines, while bending in DWTT produces only a one-dimensional stress field. Therefore, fracture development inside thickness (surface tunnelling) can be different.[16] The local necking that reduces thickness may be not the same. Finally, the plastic compression induced by the hammer can affect the fracture propagation results acquired in a DWT Tests.

Considering the effects that the constraint gives to fracture mechanics, some solutions have been presented.[17] However, no proposals were suggested to modify the DWT Tests so that the stress field matches the one experienced by pipelines, during crack running.

With the aim to gain a nominal stress field closer to the pipeline one, a new layout to perform laboratory tests on three point bending specimens is proposed. The main advantage of this new experimental set-up concerns the stress field ahead the crack tip, which now results from a bending associated with a consistent normal stress. In a DWT Test, the stress ahead the tip decreases rapidly, since the nominal stress field is enforced by pure bending. Otherwise, on cracked pipelines, the nominal circumferential stress is kept on by gas pressure. Moreover, the extension of the plastic region is obviously much wider than SENB specimen. In SENB specimens, the plasticity can reach the upper edge of the specimen only considering the local compression induced by the action of the hammer; this is to say that tensional plasticity extension is even lower than the thickness itself. This limited extension can play a misleading role when considering the effect of crack tunnelling.

The actual specimen thickness determines a constrain effect in the crack region, that induces a three-axial stress field close to the tip. The amount of the reduction of

thickness should be similar in SENB and in the pipeline, but the effective constraint applied is also governed by the stress field consistency ahead the tip.

The new layout proposed here for DWT Tests is not able to reproduce the two-dimensional nominal state of stress. However, it induces a state of stress ahead the crack tip characterized by its persistency. The distribution of the internal energy extends so that it encompasses the whole fracture process zone (FPZ). As a matter of fact, one of the limits of the DWTT is that the energy decreases inside the FPZ increasing the difficulties in the application of fracture mechanics criteria. Because the length of FPZ is higher for more ductile materials this drawback is emphasized for the new generations of pipeline steels.

Moreover, it is mandatory – to achieve reliable values for fracture parameters such as CTOA, CTOD, etc.[18] – to reach stable fracture growth. This stable fracture propagation is not easy in principle to accomplish with the DWTT layout. Without any doubt it is easier to move towards a stable growth if the nominal stress ahead the tip is consistent, as in the proposed layout. It is desirable that the critical values of the fracture parameters, identified by the proposed setup, were closer to the values to account during a fracture running in a pipeline. This can be particularly true when dealing with the new high-grade steels that exhibit noteworthy plastic deformations before rupture.

GENERAL DESCRIPTION OF THE EXPERIMENTAL SET-UP

The typical set-up of an experimental DWTT provides the measurement of the hammer load versus displacement. In such a way, the energy dissipation can be calculated through simple manipulation and time integration of the data.

DWT Tests were initially employed to gain information regarding the temperature of brittle/ductile transition. When limited to this aim, the test does not need to be instrumented since the result is obtained through the inspection of fracture aspect after test.

If the test is conducted with the help of an instrumented hammer, it is possible to compute the Crack Tip Opening Angle of the fracture during a quasi-stable propagation.[19,20]

The instrumentation here applied is also provided by a digital image recorder that automatically detects the positions of some markers, appropriately applied on the system components. The exhaustive description of the digital system of acquisition is given in Refs. [16,21]. Here, we discuss the whole procedure to gain the kinematical movements of the mechanical components, exploiting the identified locations of the markers, see Figs 1 and 2.

The description of the test is provided through the computation of a sequence of digital images taken during the advancing of the hammer. The motion of the two specimen's halves is identified during loading, even if other displacements are acting in the assembly. The plastic deformations of the specimen are concentrated on the ligament, while all other regions almost behave like rigid bodies. An exception is given by the connections of the extensions to the specimen (bolted joints), but their relative displacements, as it will be clear later on, are properly accounted in the data manipulation.

Within all pictures, every marker is localized and the taken attitudes (inclination by respect to horizontal plane) are also computed.

The system is composed by a tensile test machine, able to perform static as well as quasi-static strength tests. A couple of extensions are bolted on the edges of the SENB specimen, to lengthen the system while lowering, at the same time, the applied load. Four inclined sliding planes (supports) carry two central hinges placed at the ends of the extensions. The attitude of the supports is oriented outwards of the axis of symmetry, so that a traction is induced in the specimen while the vertical load is applied.

The peak load of the tensile test machines used (100 kN) is inadequate to carry out static DWT Tests, because it is unable to develop a bending moment capable to 'break' the specimen. The extensions are applied to reach the necessary bending moment, but they offer the considerable advantage to keep the plastic compression under the hammer very limited. Another possible solution provides the manufacturing of wider specimens directly from the pipe, but non-standard specimens result; this strategy is not advisable for the modifications induced by the flattening extended to a high circumferential portion. In such a case the flattening effective sequence can be non-univocal.

Despite the mechanical assembly, the fracture characteristics of the specimen are extrapolated from the rest; thus, the effects related to the use of extensions and inclined supports are accounted and embedded in the solution itself.

In Fig. 2, the two halves of the specimen are represented. The slope of the supports is 45°. The point W represents the intersection of the ideal – frictionless – reaction forces. The clearer markers are not located on the moving parts, so that they provide a space reference. Two darker markers are fixed on the moving halves at a considerable distance from the residual ligament; they are placed in an almost rigidly moving region. One marker indicates the hammer displacement. The remaining two darker markers are fixed on the so-called rectilinear bar that leans on the two hinges. The bar movement helps to know the actual positioning of the specimen-extensions assembly on the sliding supports.

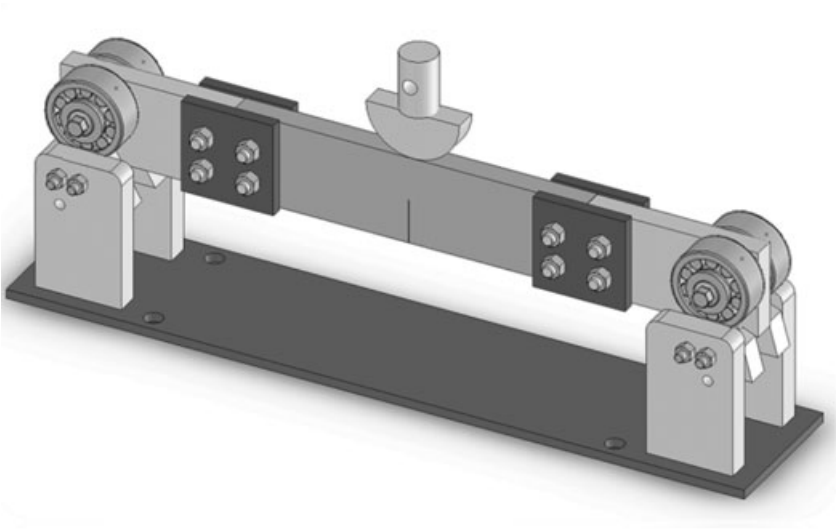

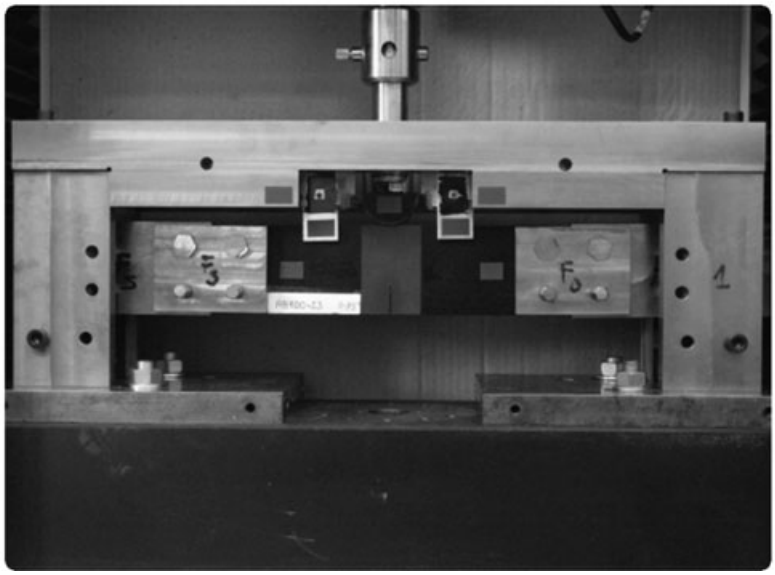

Fig. 1 Schematic view of the experimental set-up.

It is clear that, due to irreversible displacements between the ends of the specimen and the extensions (bolt connection settlements), the two bodies do not keep straight each other when load is applied.

A reference system is chosen and kept throughout the analysis; it is identified by the initial intersection between the upper surface of the specimen and the axis of symmetry.

The vertical distance from the origin of the reference system to the rectilinear bar is given by

$$_{o}f = r - \frac{H}{2} \tag{1}$$

In this reference, each marker is identified by three values: *x*-*y* coordinates of the centroid and an angle giving the horizontal attitude of the principal area axis. The position of each marker is compared with the first picture of the sequence; therefore, it is not necessary to place the markers in predefined locations, such as centroids and so on.

In a classical DWT Test, the hammer displacement is taken as the evolution parameter of the test (i.e. the reference abscissa-variable). In the proposed setup, the centres of the hinges also move; so that a new evolution parameter should be introduced. Furthermore, the extensions also rotate by respect to the specimen. For all these reasons, hereinafter the evolution parameter referenced is the average of the attitude changes of the two specimen's halves (i.e. their semi-relative rotation)

$$\delta = \frac{1}{2}[-(\theta - \theta_0)^{\mathrm{L}} + (\theta - \theta_0)^{\mathrm{R}}] \tag{2}$$

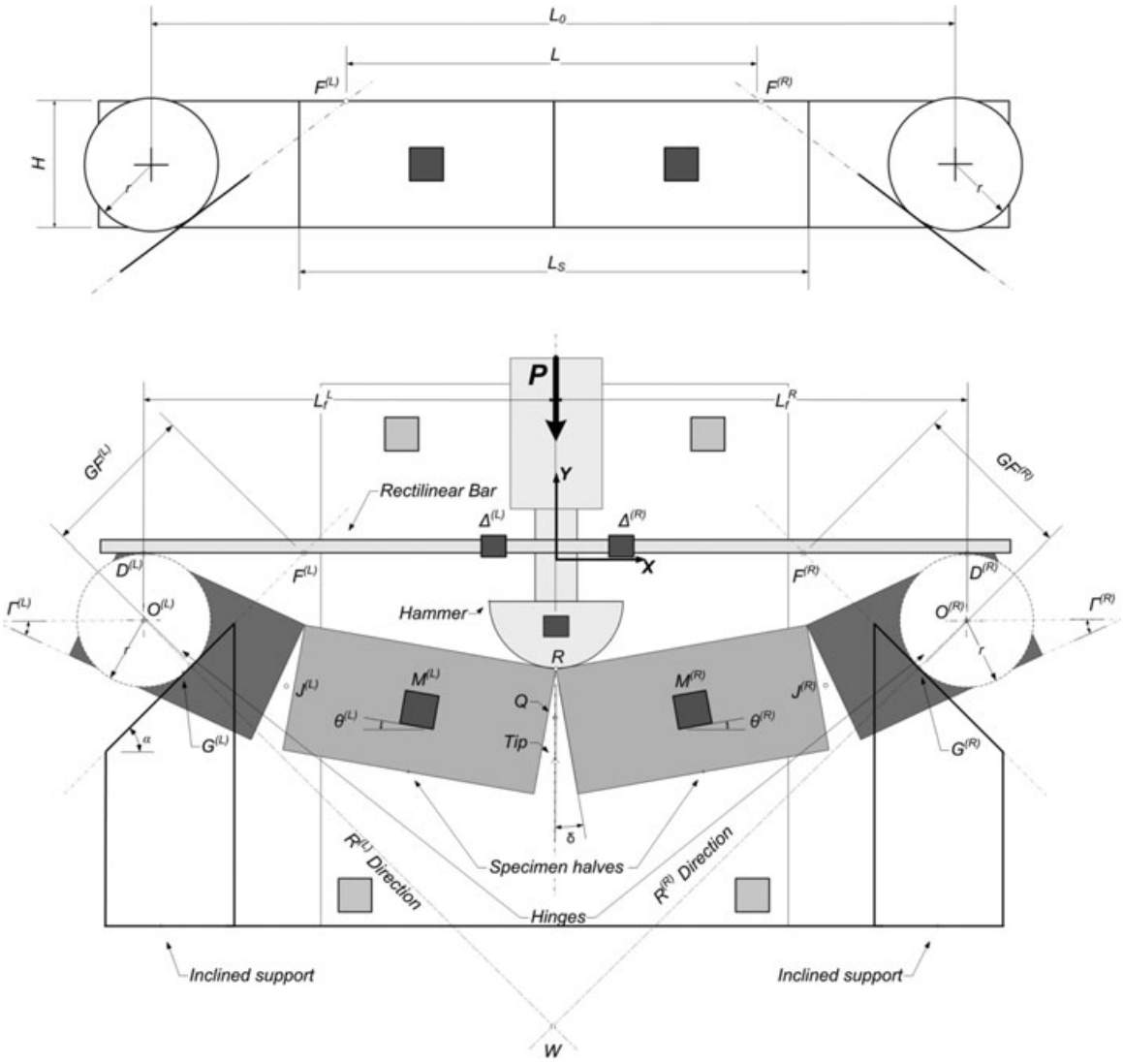

Fig. 2 Reference values on the experimental set-up.

At any time, the general attitude of the whole system, sustained by the two hinges, can deviate from the initial horizontal positioning; so that an angle (positive anti-clockwise) is computed from the displacements (referred to the first picture) of the two markers located on the rectilinear bar

$$\gamma = \arctan\left[\frac{\Delta_y^{(\mathrm{R})} - \Delta_y^{(\mathrm{L})}}{\Delta_x^{(\mathrm{R})} - \Delta_x^{(\mathrm{L})}}\right] \tag{3}$$

The vertical displacement of the rectilinear bar is computed by the search of the intersection with the y-axis (it is the same to use the left or the right marker $L|R$, but switch of sign result)

$$disp = \mp \tan(\gamma) \cdot \Delta_x^{(\mathrm{L|R})} + \Delta_y^{(\mathrm{L|R})} \tag{4}$$

The knowledge of the movements of these two markers helps to get the effective points of contact between the rectilinear bar and the two hinges.

To get these contact points, it is first necessary to explicit the distance between the intersection of the two sliding supports and the origin of the reference system (points $F^{(R)}$ and $F^{(L)}$ in Fig. 2)

$$L = L_0 - 2 \cdot \frac{r}{\tan(\alpha/2)} \tag{5}$$

where r represents the hinge radius.

If, during the test, symmetry is not preserved by the two halves, a non-negligible γ occurs. In such a case, the distances L_f between the left or right points D (where the rectilinear bar touches the hinges) and the initial axis of symmetry is not the same. According to the positive

anticlockwise choice, the respective values are

$$L_f^{(\mathrm{L,R})} = \frac{r}{\tan\left(\frac{\alpha \mp \gamma}{2}\right)} \pm \frac{disp}{\sin(\gamma)} + \frac{\left[\mp disp + \frac{L}{2}\tan(\alpha)\right]}{\sin(\alpha \mp \gamma)}\cos(\alpha) \tag{6}$$

Due to both the rectilinear bar attitude (γ) and the vertical displacement (*disp*), the coordinates of the contact points between the two hinges and the rectilinear bar are

$$\begin{cases} x_D^{(\mathrm{L})} = -L_f^{(\mathrm{L})}\cos(\gamma) \\ y_D^{(\mathrm{L})} = y_{D_0}^{(\mathrm{L})} + \frac{\Delta_y^{(\mathrm{R})} + \Delta_y^{(\mathrm{L})}}{2} + L_f^{(\mathrm{L})}\tan(\gamma) \end{cases} \tag{7}$$

$$\begin{cases} x_D^{(\mathrm{R})} = L_f^{(\mathrm{R})}\cos(\gamma) \\ y_D^{(\mathrm{R})} = y_{D_0}^{(\mathrm{R})} + \frac{\Delta_y^{(\mathrm{R})} + \Delta_y^{(\mathrm{L})}}{2} - L_f^{(\mathrm{R})}\tan(\gamma) \end{cases}$$

At this stage, the fundamental information to know are the actual location of the hinges and the contact points between the hinges themselves and the sliding supports.

The left and right distances between the hinge-support contacts and the rectilinear bar (undeformable but generally non-horizontal) are

$$\overline{GF}^{(\mathrm{L})} = \frac{r}{\tan\left(\frac{\alpha-\gamma}{2}\right)} \qquad \overline{GF}^{(\mathrm{R})} = \frac{r}{\tan\left(\frac{\alpha+\gamma}{2}\right)} \tag{8}$$

Note also that the two left and right triangles $G\hat{F}D$are isosceles so that $\overline{DF} = \overline{GF}$ (Fig. 3). The two straight lines touching points F and G have, respectively, the following parameters:

$$\begin{cases} m_{\bar{G}\bar{F}}^{(\mathrm{L})} = \tan(\alpha); \quad m_{\bar{G}\bar{F}}^{(\mathrm{R})} = -\tan(\alpha) \\ q_{\bar{G}\bar{F}}^{(\mathrm{L,R})} = -m_{\bar{G}\bar{F}}^{(\mathrm{L,R})} \cdot x_B^{(\mathrm{L,R})} + y_B^{(\mathrm{L,R})} \end{cases}$$

$$\begin{cases} m_{bar} = \tan(\gamma) \\ q_{bar} = -m_{bar} \cdot x_D^{(\mathrm{L})} + y_D^{(\mathrm{L})} \end{cases} \tag{9}$$

where m_{GF}, q_{GF}, m_{bar} and q_{bar} are slopes and y-intercepts for the $\overline{GF}$and the rectilinear bar.

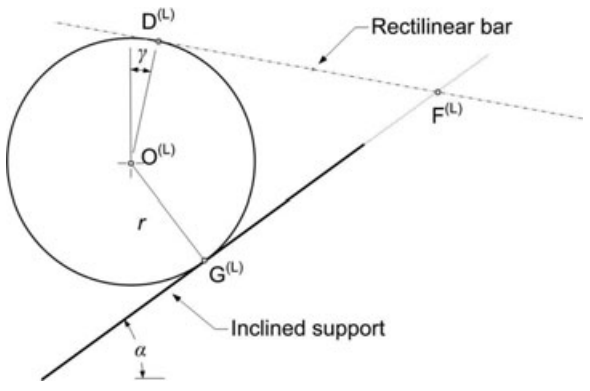

Fig. 3 Overexposure of hinge-support contact region.

The resulting coordinates of left and right points F, are

$$\begin{cases} x_F^{(\mathrm{L,R})} = \dfrac{\left(q_{\bar{G}\bar{F}}^{(\mathrm{L,R})} - q_{bar}\right)}{\left(m_{bar} - m_{\bar{G}\bar{F}}^{(\mathrm{L,R})}\right)} \\ y_F^{(\mathrm{L,R})} = m_{bar} \cdot x_F^{(\mathrm{L,R})} + q_{bar} \end{cases} \tag{10}$$

Finally, the contact points between the hinges and the rectilinear bar are now properly computed

$$\begin{cases} x_G^{(\mathrm{L})} = x_F^{(\mathrm{L})} - \dfrac{r\cos(\alpha)}{\tan\left(\frac{\alpha-\gamma}{2}\right)} \\ y_G^{(\mathrm{L})} = y_F^{(\mathrm{L})} - \dfrac{r\sin(\alpha)}{\tan\left(\frac{\alpha-\gamma}{2}\right)} \end{cases} \quad \begin{cases} x_G^{(\mathrm{R})} = x_F^{(\mathrm{R})} + \dfrac{r\cos(\alpha)}{\tan\left(\frac{\alpha+\gamma}{2}\right)} \\ y_G^{(\mathrm{R})} = y_F^{(\mathrm{R})} - \dfrac{r\sin(\alpha)}{\tan\left(\frac{\alpha+\gamma}{2}\right)} \end{cases} \tag{11}$$

Moreover, the actual locations of the centres of the two hinges are given by the two couples of coordinates, respectively,

$$\begin{cases} x_O^{(\mathrm{L})} = x_F^{(\mathrm{L})} - r\left[\cot\left(\dfrac{\alpha-\gamma}{2}\right)\cos(\gamma) + \sin(\gamma)\right] \\ y_O^{(\mathrm{L})} = y_F^{(\mathrm{L})} - r\left[\cot\left(\dfrac{\alpha-\gamma}{2}\right)\sin(\gamma) - \cos(\gamma)\right] \end{cases}$$

$$\begin{cases} x_O^{(\mathrm{R})} = x_F^{(\mathrm{R})} + r\left[\cot\left(\dfrac{\alpha+\gamma}{2}\right)\cos(\gamma) + \sin(\gamma)\right] \\ y_O^{(\mathrm{R})} = y_F^{(\mathrm{R})} - r\left[\cot\left(\dfrac{\alpha+\gamma}{2}\right)\sin(\gamma) + \cos(\gamma)\right] \end{cases} \tag{12}$$

In the same reference system, the effective fracture tip should be located at every frame. The effective ligament (*Lig*) is known thanks to a different algorithm applied on digital images. It identifies the distance between the point where the load is applied and the crack tip as it appears on the surface. In a brief synthesis, the algorithm identifies the crack tip through an extrapolation of a simple polynomial that fits the crack flanks. [22]

The moving markers ($M^{(\mathrm{L|R})}$) attached on the specimen's halves are positioned with a 'rule of thumb'; however, taking advantage of the identification of the markers at the first picture (unloaded), one can precisely compute the effective marker locations on the specimen. An eventual asymmetrical initial disposition of the markers (typically 1 mm uncertainty) is *a priori* corrected by a rigid motion assumption; therefore, we assume a perfect symmetry of the two halves for an easy writing of the subsequent equations. With this statement in mind, the coordinates of mobile markers are given as simple incremental quantities.

As mentioned before, a mobile marker is located on the hammer head, its movement gives the deflection of the specimen and its coordinates are said R_x and R_y.

In the reasonable hypothesis that the centre of contact on the hammer can only move in the y-direction, by the knowledge of the marker locations and ligament value,

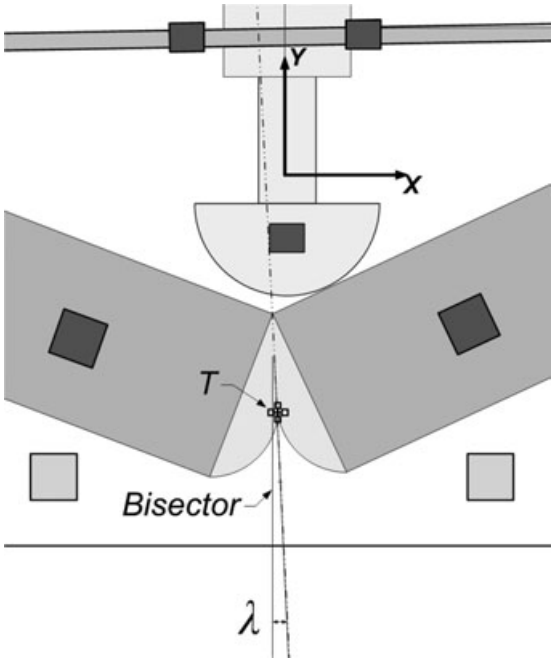

Fig. 4 Crack tip location in the Reference System.

one obtains the actual coordinates of the crack tip (point T in Fig. 4)

$$\lambda = \arctan\left(\frac{y_M^{(\mathrm{R})} - y_M^{(\mathrm{L})}}{x_M^{(\mathrm{R})} - x_M^{(\mathrm{L})}}\right) \quad \begin{cases} T_x = 0 + Lig \cdot \sin\lambda \\ T_y = R_y + Lig \cdot \cos\lambda \end{cases} \tag{13}$$

It is important to highlight that the angles λ (measuring the asymmetry of the two specimen halves) and γ (measuring the rectilinear bar horizontal attitude) are not the same, as shown in Fig. 5. This is due to the relative rotations between the two ends of the specimen and the two extensions connected by bolts (*de facto* they can be different in the left and right sides).

At this stage, the kinematical features of the event are defined at each frame. All previously given quantities are necessary to force the equilibrium conditions, i.e. computing the loads actually applied on the specimen.

Within this experimental setup, all surfaces in contact of the system are rolling elements, this means that friction is present, but friction loads are much smaller than reaction loads. According to this, it is supposed that the reaction forces on the inclined supports are orthogonal to them. All existing friction loads are considered concentrated in the hammer contact. Taking advantage of the previous coordinates of points $O^{(\mathrm{L|R})}$ at left and right, respectively, the straight lines containing the reaction loads have the following parameters in the Reference System:

$$\begin{cases} m_{\bar{G}\bar{O}}^{(\mathrm{L,R})} = \dfrac{y_O^{(\mathrm{L,R})} - y_G^{(\mathrm{L,R})}}{x_O^{(\mathrm{L,R})} - x_G^{(\mathrm{L,R})}}; \\ q_{\bar{G}\bar{O}}^{(\mathrm{L,R})} = -m_{\bar{G}\bar{O}}^{(\mathrm{L,R})} \cdot x_G^{(\mathrm{L,R})} + y_G^{(\mathrm{L,R})} \end{cases} \tag{14}$$

The two lines intersect each other at point W (Fig. 2); here the lever arms of the constrain loads are both zero, its coordinates are

$$\begin{cases} x_w = \dfrac{q_{\bar{G}\bar{O}}^{(\mathrm{R})} - q_{\bar{G}\bar{O}}^{(\mathrm{L})}}{m_{\bar{G}\bar{O}}^{(\mathrm{L})} - m_{\bar{G}\bar{O}}^{(\mathrm{R})}} \\ y_w = m_{\bar{G}\bar{O}}^{(\mathrm{R})} \cdot x_w + q_{\bar{G}\bar{O}}^{(\mathrm{R})} \end{cases} \tag{15}$$

Now, for the computation of the friction load acting on the hammer head, the point W is used as the centre of rotation for the equilibrium. The point of application of the load is always on the axis of symmetry, but the direction of the friction load is assumed on the specimen half that intersects the axis of symmetry (intersecting half).

At point W, the reaction loads have not any resulting moment, the vertical load lever arm is simply the x-coordinate of point W. The lever arm of the friction load is computed considering the plane containing the upper surface of the intersecting specimen half

$$Lev_{Frict}^{(\mathrm{L|R})} = \frac{|y_W \pm \tan(\theta - \theta_0)^{(\mathrm{L|R})} x_W - R_y|}{\sqrt{1 + \tan^2(\theta - \theta_0)^{(\mathrm{L|R})}}} \tag{16}$$

The alternative symbol $L|R$ and signs indicate whether the point W results on the right of the axis of symmetry or on its left. Finally, the friction load is given by

$$\mathbf{F}_{Frict}^{(\mathrm{L|R})} = \pm \frac{|x_w|}{Lev_{Frict}} \mathbf{P} \tag{17}$$

The lines of action of the reaction loads are given, but it is also essential to know the reaction values to compute the effective loads applied on the ligament section. Making the moment equilibrium by respect to centres $G^{(\mathrm{L,R})}$, one obtains

$$\mathbf{R}^{(\mathrm{R,L})} = \frac{x_G^{(\mathrm{L,R})} \cdot \mathbf{P} + \dfrac{\left| y_G^{(\mathrm{L,R})} - \tan(\theta - \theta_0)^{(\mathrm{L,R})} x_G^{(\mathrm{L,R})} - R_y \right|}{\sqrt{1 + \tan^2(\theta - \theta_0)^{(\mathrm{L,R})}}} \cdot \mathbf{F}_{Frict}}{\sin(2\alpha)\sqrt{\left(x_W - x_G^{(\mathrm{L,R})}\right)^2 + \left(y_W - y_G^{(\mathrm{L,R})}\right)^2}} \cdot \tag{18}$$

Despite the presence of the inclined supports, the plastic energy absorbed by the simple traction of the specimen is very small if compared to the energy absorbed by the plastic hinge rotation. This assumption will be confirmed later on in the paper, when some experimental data are discussed.

Therefore, the attention is focused on the rotation of the plastic hinge as the main mechanism that causes the

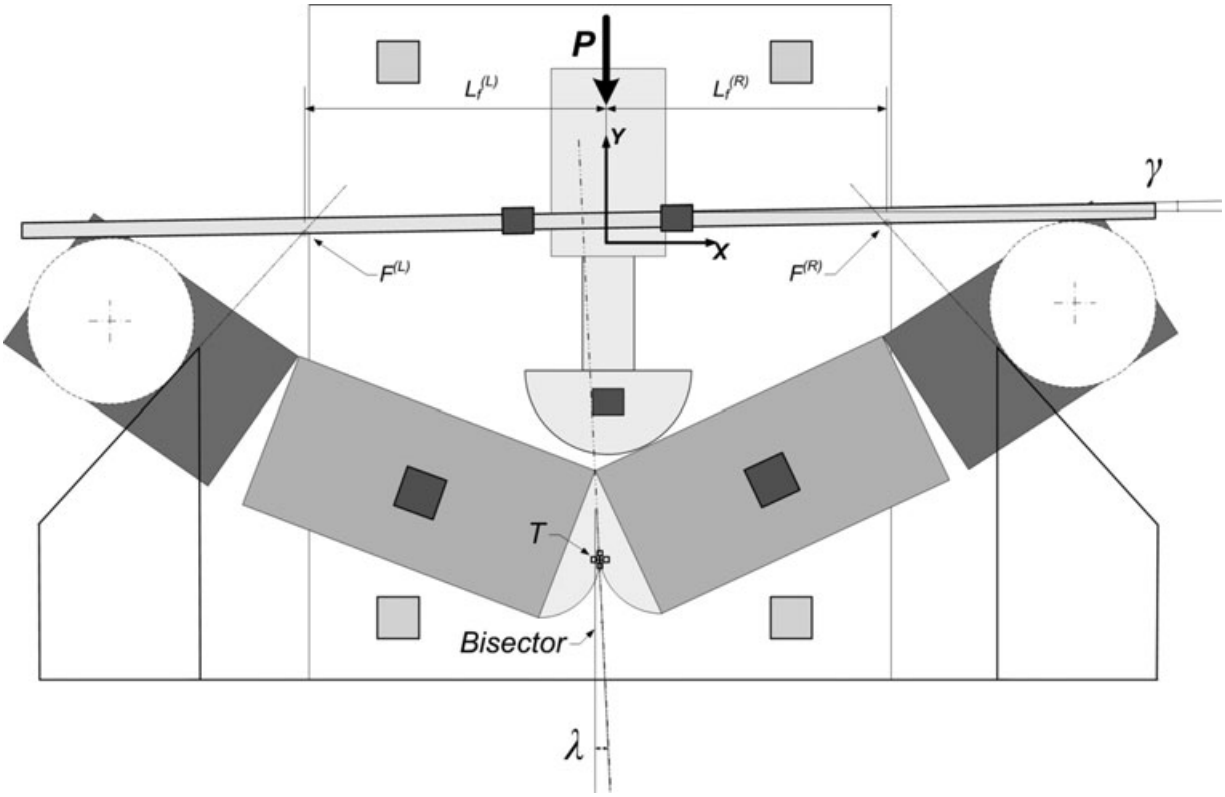

Fig. 5 Non-balanced attitude of the system during test.

fracture advancement in the specimen. According to this point of view, we can join data coming from tests that have a different support slope α.

We are interested to the generalized loads acting on the ligament section. Any point of the section could be used for it; here, for simplicity, the loads are accounted at the centre of the actual ligament Q (Fig. 2).

It is possible to compute the longitudinal stretch experienced at the ligament section of the specimen; its value corresponds to the difference between the effective marker positions and those computed through simple rotations around point Q

$$flow^{(\mathrm{L,R})} = \mp\left[M_x^{(\mathrm{L,R})}\sin(\theta-\theta_0)^{(\mathrm{L,R})} + M_x^{(\mathrm{L,R})}\cos(\theta-\theta_0)^{(\mathrm{L,R})}\right] - \left(M_x^{(\mathrm{L,R})} - x_Q\right) \tag{19}$$

At the centre Q, the resulting moment is

$$\mathbf{M}_{Lig} = \left[\pm\mathbf{R}^{(\mathrm{L|R})}\sin(\alpha)\cdot\left(y_G^{(\mathrm{L|R})} - y_Q\right) + \mathbf{R}^{(\mathrm{L|R})}\cos(\alpha)\cdot\left(x_G^{(\mathrm{L|R})} - x_Q\right)\right] - \left|\mathbf{F}_{Frict}\cdot\frac{Lig}{2}\right| \tag{20}$$

Figure 6 helps for the orientation of the friction load on the specimen surface and refers to the case of its positioning on the right. The resulting axial load is

$$\mathbf{F}_{Lig} = \mathbf{R}^{(\mathrm{R|L})}\sin(\alpha) = \mathbf{R}^{(\mathrm{L|R})}\sin(\alpha) + \mathbf{F}_{Frict}^{(\mathrm{R|L})}\cos(\delta\pm\gamma) \tag{21}$$

For the accounting of the energy dissipated at the bolted connections between the specimen ends and the

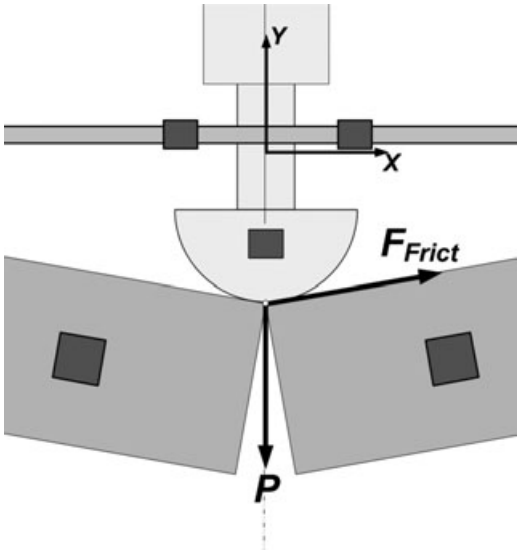

Fig. 6 Effective direction assumed by the friction force.

extensions, it is possible to derive the relative rotations. It is assumed that the joints can only be affected by a rotation located at the geometric centre of the two plaques connecting the two parts (see Fig. 1).

The coordinates of these central points are (Fig. 2)

$$\begin{cases} x_{\mathcal{J}}^{(\mathrm{L,R})} = x_M^{(\mathrm{L,R})} \mp \dfrac{L_s}{4}\cos(\delta^{(\mathrm{L,R})}) \\ y_{\mathcal{J}}^{(\mathrm{L,R})} = y_M^{(\mathrm{L,R})} - \dfrac{L_s}{4}\sin(\delta^{(\mathrm{L,R})}) \end{cases} \tag{22}$$

where $\delta^{(L,R)}$ is the rotation of the two halves, with a positive sign if rotations are anti-clockwise, and L_s is the initial length of the specimen.

The relative rotations of the two halves of the specimen and the extensions are given by

$$\Gamma^{(\mathrm{L,R})} = \arctan\left(\pm\frac{y_O^{(\mathrm{L,R})} - y_{\mathcal{J}}^{(\mathrm{L,R})}}{x_O^{(\mathrm{L,R})} - x_{\mathcal{J}}^{(\mathrm{L,R})}}\right) - \delta^{(\mathrm{L,R})} \tag{23}$$

The bending moments experienced at the extension connections are easily computed if considering the appropriate lever arm together with the reaction loads

$$\mathbf{M}_{EndCon} = \frac{-\left[\mathbf{R}^{(\mathrm{L})}\sin(\alpha)\cdot\left(y_G^{(\mathrm{L})} - y_{\mathcal{J}}\right) + \mathbf{R}^{(\mathrm{L})}\cos(\alpha)\cdot\left(x_G^{(\mathrm{L})} - x_{\mathcal{J}}\right)\right] + \left[\mathbf{R}^{(\mathrm{R})}\sin(\alpha)\cdot\left(y_G^{(\mathrm{R})} - y_{\mathcal{J}}\right) + \mathbf{R}^{(\mathrm{R})}\cos(\alpha)\cdot\left(x_G^{(\mathrm{R})} - x_{\mathcal{J}}\right)\right]}{2} \tag{24}$$

From all previous kinematical and dynamical results, all energies involved in the test can be derived

- Total energy put in the system: $E_{TOT} = \sum_{i=2}^{npict} \mathbf{P}(i)\cdot[\mathbf{R}_y(\mathbf{i}) - \mathbf{R}_y(\mathbf{i-1})]$
- Energy of the bending at the ligament section:

$$E_{Lig} = \sum_{i=2}^{npict} \mathbf{M}_{Lig}(i)\cdot[\delta(i) - \delta(i-1)] \tag{25}$$

- Energy lost in the specimen connections: $E_{EndCon} = \sum_{i=2}^{npict} \mathbf{M}_{EndCon}(i)\cdot[\Gamma(i) - \Gamma(i-1)]$
- Energy lost in overall frictions: $E_{Fricit} = \sum_{i=2}^{npict} \mathbf{F}_{Fricit}(i)\cdot Le\,v_{Fricit}(i)\cdot[\delta(i) - \delta(i-1)]$
- Energy associated to longitudinal stretch: $E_{Flow} = \left[\sum_{i=2}^{npict} \mathbf{R}^{(\mathrm{L})}\sin(\alpha)\,flow^{(\mathrm{L})} + \mathbf{R}^{(\mathrm{R})}\sin(\alpha)\,flow^{(\mathrm{R})}\right]$

COMBINED TEST

One of the important drawbacks, connected with the use of inclined supports is that, when the slope is set to high values and the crack has not yet started moving, the reaction loads can reach considerable values. To get around this difficulty, we explored the possibility to subdivide the test into two phases.

In the first phase, the load is applied on non-inclined supports ($\alpha = 0^\circ$) until the crack starts to have a stable propagation. This occurs when the load has reduced almost to half its maximum value. This condition is experimentally chosen when the relative rotation of the two specimen halves reaches a fixed value. After that, the test is suspended, the specimen is remounted on the desired inclined supports and the test is restarted. This split procedure allows the use of very inclined supports, thus approaching the effective persistent state of stress that is experienced in front of a crack running on a pipeline. This type of procedure is herein called *combined test*.

To make it evident the advantages embedded in the use of inclined supports, we performed some Finite Element analyses on the specimen subjected to large plasticity and deflections, mounted on differently inclined supports.

There is no need here to model also the bolted connections, so that the model consists of a specimen as long as 545 mm with a *12 mm* initial indentation. The model is meshed with 12880 solid elements and solved with an implicit Finite Element solver. This elasto-plastic analysis is focused on the size of the stress persistency region ahead the crack tip; therefore, the tunneling (non straight crack through thickness), the process zone (due to increasing damage ahead the blunting) and the crack growth, are all unconsidered in the analysis.

The results are shown in Fig. 7. Here the normalized stresses along the ligament for five different DWTT inclined configurations (0°, 45°, 60°, 75°, 85°) are shown, together with the circumferential stress evaluated by the computation on a full pipeline [23] This last is evaluated according to an explicit Finite Element code, suitably developed for this kind of application.[24]

The normalization to the flow stress value does not make it evident the difference due to *T-stress* in the two models that is, as a matter of fact, present. However, it is clear that the Fracture Process Zone [22,25] of the pipeline (on the order of the thickness value) surely extends on a region of persistent circumferential stress. This happens in the Three Point Bending specimens only if the slope of the inclined supports reaches values well above 60°.

In other words, the neutral axis position moves the more and more upwards, with an increasing rate. Low angles of supports, until 60°, are not enough to realize the persistent tensile stress on the specimen, and therefore to suitably modify the stress distribution on the ligament.

In the combined tests, all the above formulations are yet valid, but there is the need to adjust the post processing phases, getting an appropriate correlation of the data collected in the two subdivided steps. The strategy used to combine the two steps is centred on the relative rotation of the two halves of the specimen, rather than on the displacement of the hammer. The data of the second step are

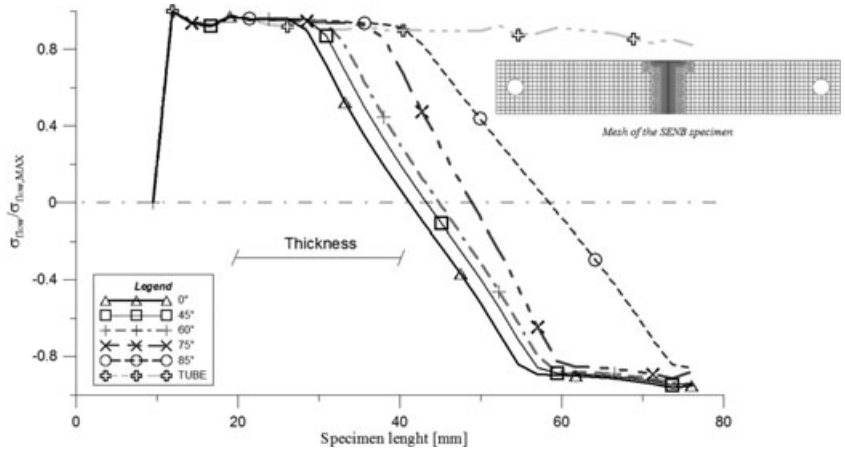

Fig. 7 Stress trend on the ligament for some support angles.

queued to the data of the first one, so that a continuous and monotonic trend in the rotation of the specimen is achieved. The step switch is planned so that the stable propagation of the crack happens almost entirely when the supports are inclined.

It is necessary to introduce a rigid shift on the marker location (since it is really impossible to reposition the specimen in the same location when restarting the test), so that the first configuration of the second step overlaps with the last configuration of the first one.

Therefore, any marker is subjected to appropriate shifts and rotation.

$$Shift_x = R_x^{\text{First}}(end) - R_x^{\text{Second}}(cut) \tag{26}$$

$$Shift_y = displ^{\text{First}}(end) - displ^{\text{Second}}(cut) - \frac{\left(\Delta_y^{(\text{L})}(cut) + \Delta_y^{(\text{R})}(cut) \cdot \dfrac{\Delta_x^{(\text{R})}(1)}{\Delta_x^{(\text{L})}(1)}\right)}{\left(1 + \dfrac{\Delta_x^{(\text{R})}(1)}{\Delta_x^{(\text{L})}(1)}\right)} \tag{27}$$

$$Shift_\delta = \gamma^{\text{First}}(end) - \gamma^{\text{Second}}(cut) \tag{28}$$

The initial distance between the external hinges is no more equal to L_0, since it should consider the displacements occurred in the first step, that is to say, the rotations on the ligament and those on the bolted connections

$$L_0^{\text{CT}} = L_S \cdot \cos(\delta_{in}) + (L_S - L_0) \cdot \cos\left(\frac{\Gamma^{(\text{R})} + \Gamma^{(\text{L})}}{2} + \delta_{in}\right) \tag{29}$$

When reloading the specimen during the second step, it is necessary to identify the frame in which the relative rotation of the two halves is just higher than the final value experienced in the first step, we label this frame as *cut*.

When the above conditions are fulfilled, the estimation of all energy rates belonging to the two experimental steps is combined together. Being energy an incremental quantities, previous eq.s (25) become:

$$E_i = \begin{bmatrix} E_I \begin{bmatrix} 1 \\ \vdots \\ end_I \end{bmatrix} \\ E_{II}\left(E_I(end_I) + \begin{bmatrix} cut \\ \vdots \\ end_{II} \end{bmatrix}\right) \end{bmatrix} \text{ with} \tag{30}$$

$$i = [TOT, Lig, EndCon, Frict, Flow]$$

EXPERIMENTAL MEASUREMENTS

The experimental data here discussed are relative to a maximum value of the support inclination equal to 60°. Even if it is clear, by Fig. 7, that the full satisfaction of the persistency of the stress ahead the crack is fulfilled only above 60°, here it is important to highlight that the measurements carried on with inclined supports can be successfully compared with the standard DWTT, if relative rotations are considered like the evolution parameter. The comparison among differently-inclined support tests, all together, helps to have an insight of how representative are the fracture features deduced by DWT Test (rapidly-decreasing nominal stress field) of fractures running on pipelines where persistent stress fields act in the fracturing region.

The limit on the support slopes is due to the inadequate structural stiffness of the present prototypal set-up. A new experimental set-up that can operate with supports up to 85° is under testing. However, we can claim that the stress persistency has a remarkable effect on crack growth.

In Fig. 8 it is shown, for the X100 specimens, the effective ratio between two nominal stresses: the stress due to horizontal loads given by support reactions and the hoop stress in a pipeline taken as the 75% of the yield stress.

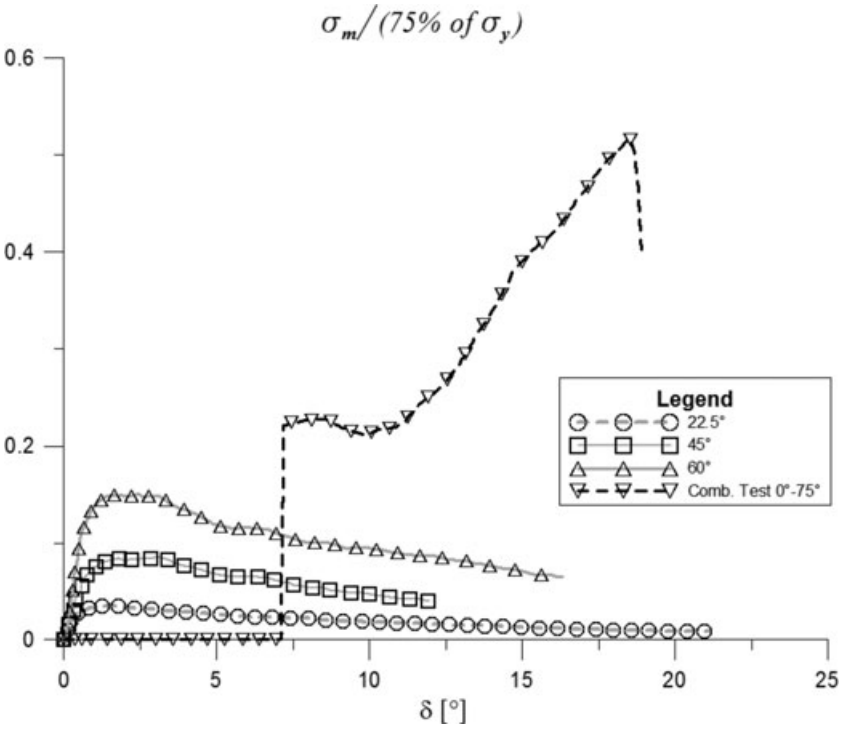

Fig. 8 Effective additional stress normalized on 75% of the yielding stress.

The ratio increases with the inclination of the supports. Note that very high values (comparable to hoop stress in the pipeline) can be reached when the inclined supports is set to 75°. This test data are drawn by the first experiments conducted with the new set-up but other results are still under investigation. The whole procedure discussed in the previous section is helpful for both set-up, the prototypal one here used for the presented results and the upgraded one whose results are not ready for a satisfactory presentation.

The overall horizontal loads, which are generated by a slope higher than 60°, are such that the combined test procedure is mandatory. Therefore, the computational changes induced by this approach have been applied to the prototypal set-up.

The stress field experienced by the region near the crack tip in a gas pipeline is very complex. The ratio between the diameter and the thickness allows to assume a nominal state of plane stress. The constrain effect due to thickness can be ignored far away the fracture tip, but its contribute is very remarkable close to the tip, where a tri-axial stress distribution occurs. Moreover, by full scale burst tests of buried pipelines, an important longitudinal strain of the pipe is generated by an additional stress component in the longitudinal direction .[21] The suggested experimental layout is not able to reproduce on a SEN-B specimen all these components of the stress; however, it represents an important improvement. It extends the stress distribution along the ligament and expands the part of the test characterized by stable fracture-propagation.

By a practical point of view, the combined test is carried out performing two consecutive experiments. Some inaccuracies due to the assembling and subsequent disassembling of the entire experimental set-up are unavoidable. An interesting solution foresees the adoption of supports having a varying slope, such as to ensure the wished change of the direction of the reaction forces, thus overcoming the necessity to divide the experiments in two subsequent steps.

EVALUATION OF THE PRESENT EXPERIMENTAL SET-UP PERFORMANCES

The different slope of the supports determines a modification on the kinematics of the test. In the standard DWT Test the specimen is supported by two rigid hemicylindrical contact surfaces. In the present experimental set-up the specimen is hold on two circular hinges centred on its middle height, which can slide on inclined supports.

As above mentioned, it is preferable to analyze the experimental results through the relative rotation of the specimen halves rather than the longitudinal displacement of the hammer.

To this regard, it is useful to analyze the results given in Fig. 9, which shows the hammer-load versus

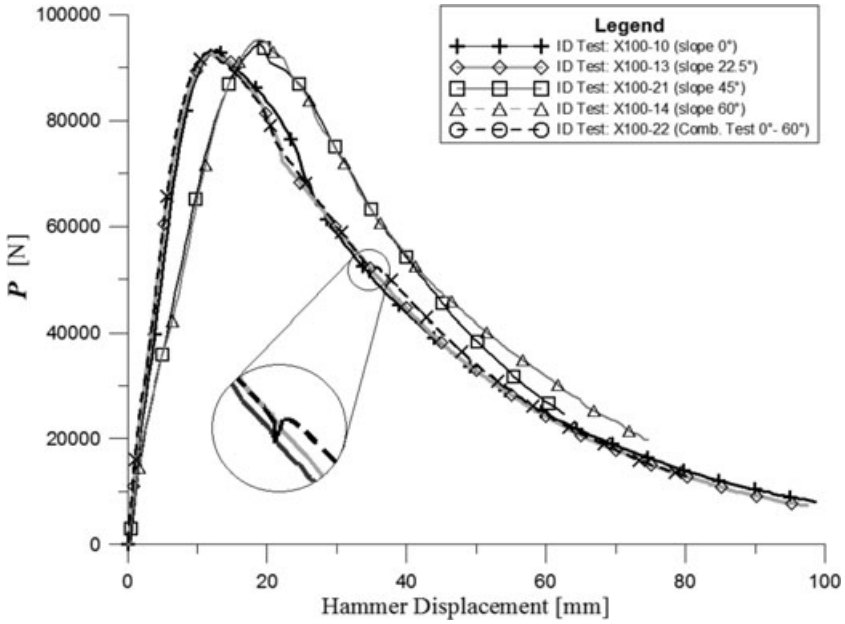

Fig. 9 Hammer load-displacement for X100 specimens.

hammer-displacement for five slopes of the inclined supports. The tests are carried out on X100 SEN-B specimens with *21 mm* thickness and *25 mm* of initial indentation. The plotted curves are all characterized by the same peak load, but their shapes are not the same. In the same figure, two families of curves can be single out: low support angles (0°; 22.5°) and high support angles (45°; 60°). This scattering is originated by the difference in the motion of the hinges, whose vertical displacements are the more and more important as the support slopes increase.

This assertion is confirmed by the Combined Test, which shows a discontinuity of trend in correspondence of the point where the support slope is changed (see small circle in Fig. 9): from this point onwards the curve becomes closer to the high-angle group. Following the indications given by Fig. 9, one can foresee an even more accentuated increase for higher inclinations of the supports. This makes it impossible to join together experimental results collected with a different inclination of the supports. If one represents the bending moment acting at the centre of the specimen, by respect to the relative rotations of the specimen halves, it is possible to overcome this drawback (see Fig. 10).

All tests, regardless of the support slope, show the fracture propagating at the same conditions, i.e. the same combinations of bending, in the ligament section, and rotation of the two specimen halves. All data are almost superimposed on Fig. 10. It is important also to highlight that, by this point of view, the discontinuity observed in the combined test vanishes.

The results shown in Figs 9 and 10 also confirm the numerical results plotted in Fig. 7. Up to 60° of the support slope the effect of the stress persistency is hard to remark, that is to say that the work of fracture is not affected by the slope itself. According to all above considerations, one could claim that, whether some differences will be found when adopting higher support slopes, these differences could be ascribed to a different behavior of the propagating fracture. This behavior is anyhow closer to fracture propagation in pipelines.

The Fig. 11 shows the total energy put in the specimen, through the work done by the hammer, for five different slopes of the supports (0°, 22.5°, 45°, 60° and combined 0°-60°).

Two curve families can be distinguished according to the different trend of the energy; the first one encompasses the tests carried on with the lower slopes and the combined one (0°, 22.5°, combined 0°-60°), the second one encompasses the higher slopes (45°,60°).

If the same comparison is performed using the sum of all the energies previously computed by eqs (25) (E_{Lig}, E_{Frict}, E_{Flow}, E_{EndCon}) all curves get closer (Fig. 12).

The surplus given by these discrepancies is not ascribed to a wrong use of eqs (25), but it is the result of an addictive term, direct consequence of the deformabilities of the experimental apparatus when the higher loads are reached.

When the supports are highly inclined, some huge horizontal loads act on the supporting frame, and a considerable energy is absorbed by the structure itself, especially in the first part of the test, when the highest hammer loads are applied. To this purpose it is interesting to point out the discontinuity observed in the combined test of Fig. 11 (a small circle helps the identification) that shows a small but sudden increase of the energy put in the system. To further reinforce this guess the same energy results are

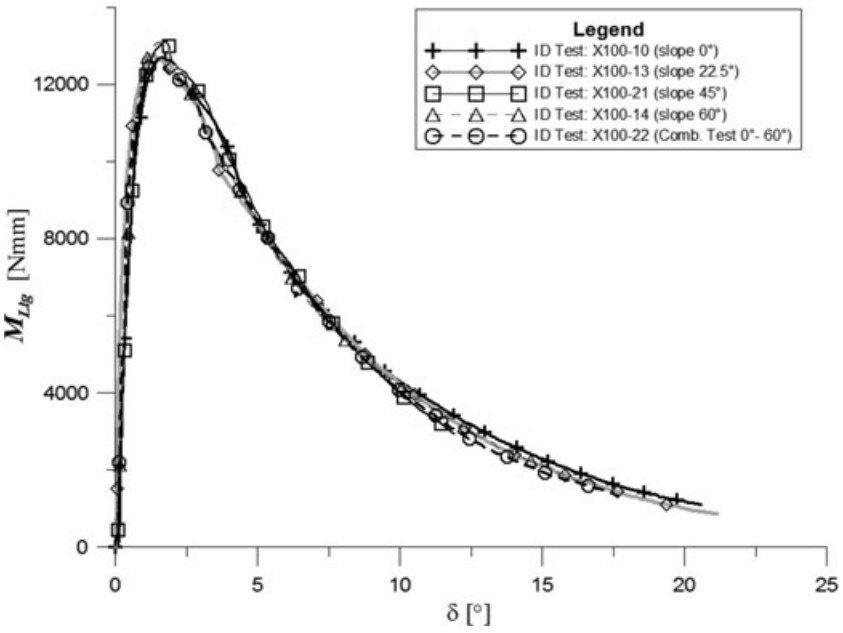

Fig. 10 Bending moment for X100 specimens versus the relative rotation between specimen halves.

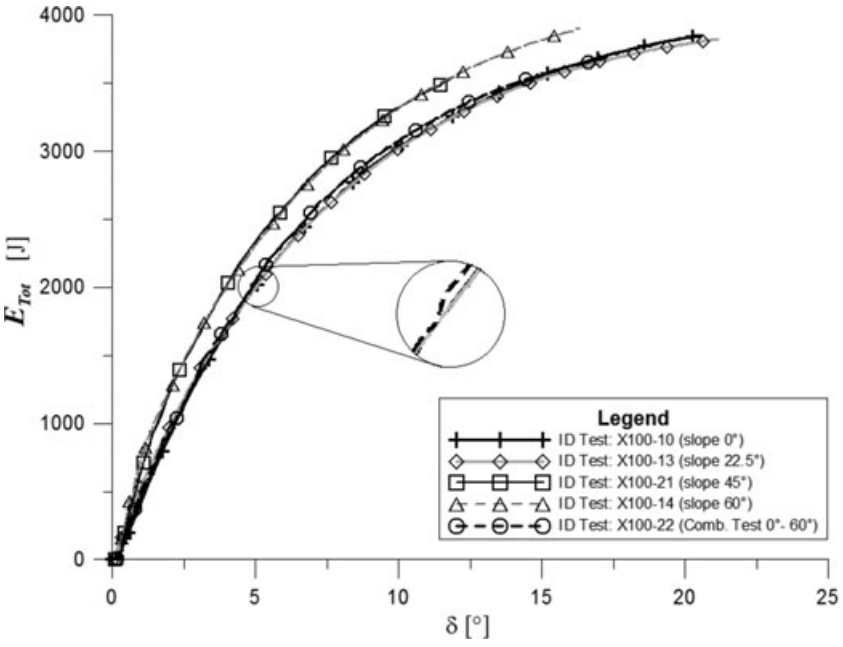

Fig. 11 Given total energy for X100 specimens.

given for the X60 material, considering the energy put in the system (Fig. 13) and the energy sum (Fig. 14). The lower strength of this material, when compared to X100, generates a much smaller disagreement between the two groups of energies, since the peak load is now almost reduced to the half.

Hereinafter, in rapid succession, the four components of the energies are discussed.

In Fig. 15 the energy data represents the work adsorbed by the rotation around the plastic hinge, close to the ligament centre; this quantity is strictly connected to the crack advance. All support slopes give the same trend. This suggests that fracture mechanism is the same, at least when the slope is not higher than 60°. Note that this result agrees with the considerations derived by the finite element analysis, reported in Fig. 7. It is also confirmed the need to adopt higher support slopes, connected to a new much stiffer frame structure.

In Fig. 16 the attention is devoted to the energy loss localized at the bolted connections between the specimens and the extensions. The measured energies reach less than one tenth of the previous E_{Lig}. The maximum values

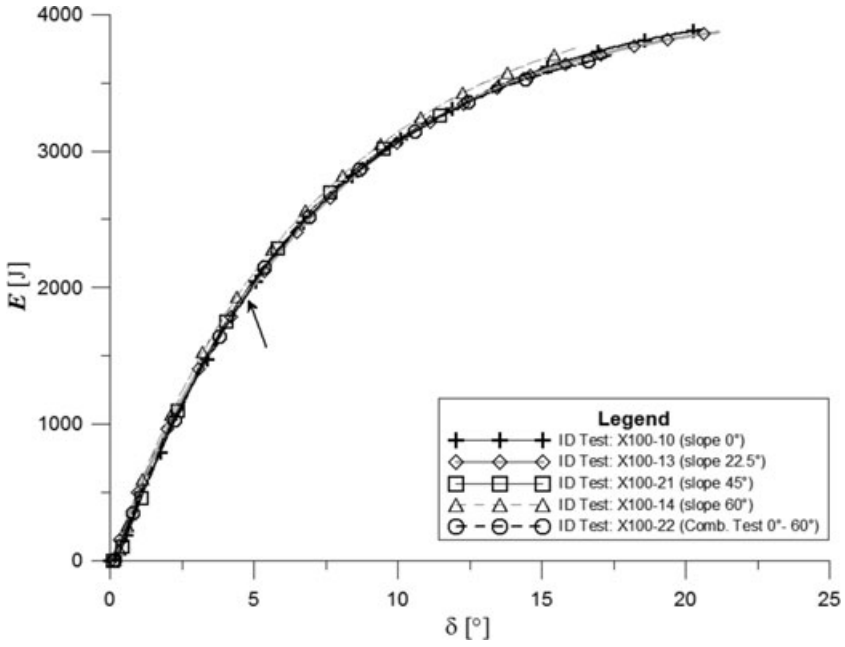

Fig. 12 Sum of all energy terms for X100 specimens.

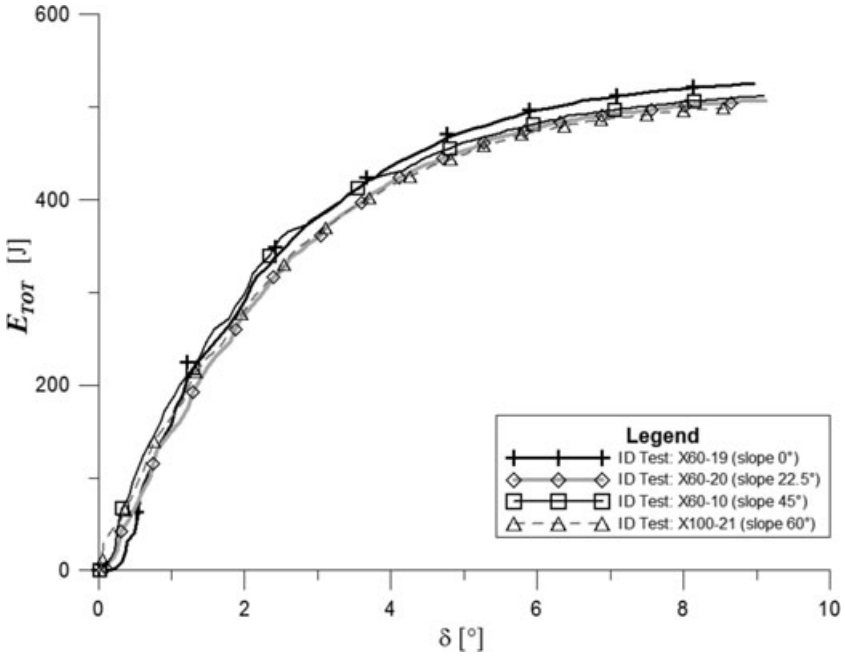

Fig. 13 Given total energy for X60 specimens.

regard the 60°-support, whose huge horizontal loads induce the adjustment and partial collapse of the bolts (or spines). A special behaviour regards the combined test, where the horizontal loads suddenly appear at the slope change. As a matter of fact, these horizontal loads have not been given in advance, during the initial preload (always performed to recuperate the clearances); therefore, the adjustment of the bolts begins only at the second phase.

In Fig. 17 the energy dissipated by friction energy loss is shown. We point out that the magnitude and direction of the friction loads result by a momentum equilibrium centered on a pole given by the intersection of the normal reaction loads on the slides. This intrinsically means that all friction loads are conceived as concentrated on the hammer surface. This is also the reason why on Fig. 17 one cannot find the data relative to 0°-support (the arm tends towards infinite). As a result of the procedure to account of friction, this last is dependent on the general attitude of the specimen-extensions (angle γ). This statement is confirmed for the 22.5°, 60°, combined-60° that in its second phase follows the simple 60°; but an exception is given by 45° whose friction energy is surprisingly higher.

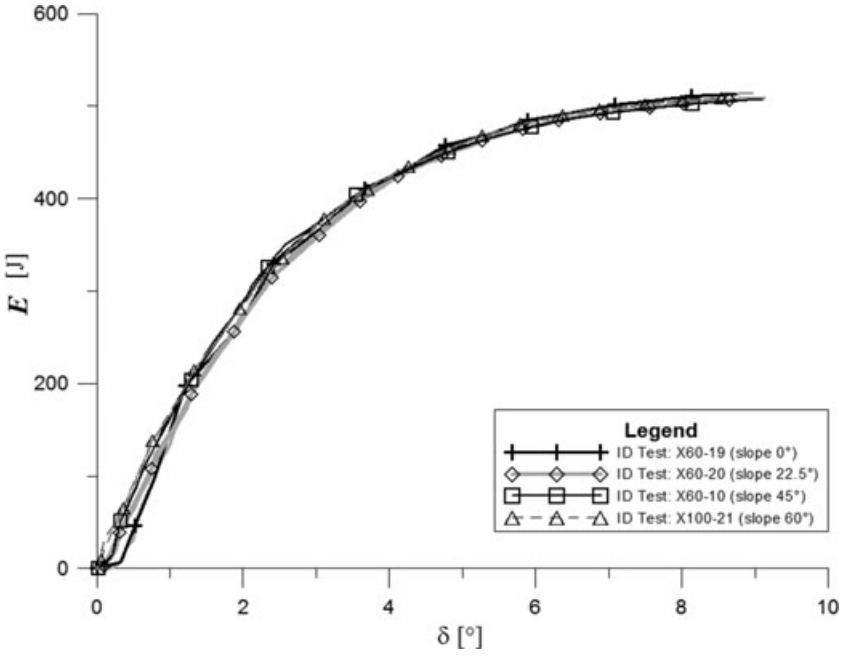

Fig. 14 Sum of all energy terms for X100 specimens.

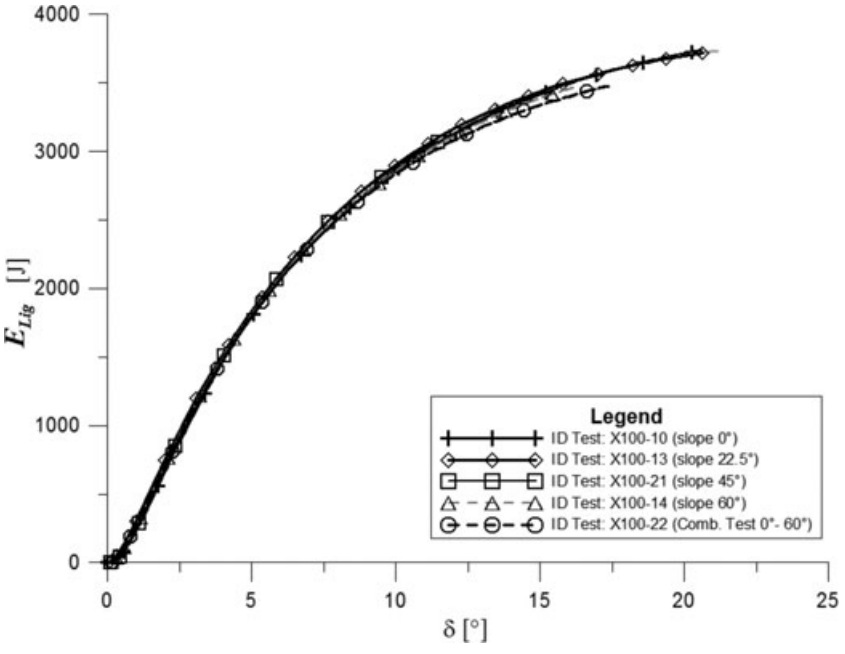

Fig. 15 Sum of all energy rates for X60 specimens.

This discrepancy is connected to the global attitude γ (see its values in Fig. 18) where the attitude relative to 45° is much more accentuated than all the others. A check of the precision of the support locations and slopes, which effectively resulted all at the same level, would exclude that the system simply recuperates misalignments. A more exhaustive motivation should be researched by means of stability analysis of the specimen-extensions, when supported on inclined slopes.

To this goal, hereinafter the kinematic stability has been analyzed. In Fig. 19 the scheme of the system containing all geometric quantities is depicted. Two configurations are considered; point–point-dotted in the unbalanced arrangement, continuous line in the configuration assumed when an angle γ occurs.

Assuming that a identifies the horizontal offset, ϑ is the complementary angle of the support slope, it is helpful to evaluate the length of the specimen by means of the sum

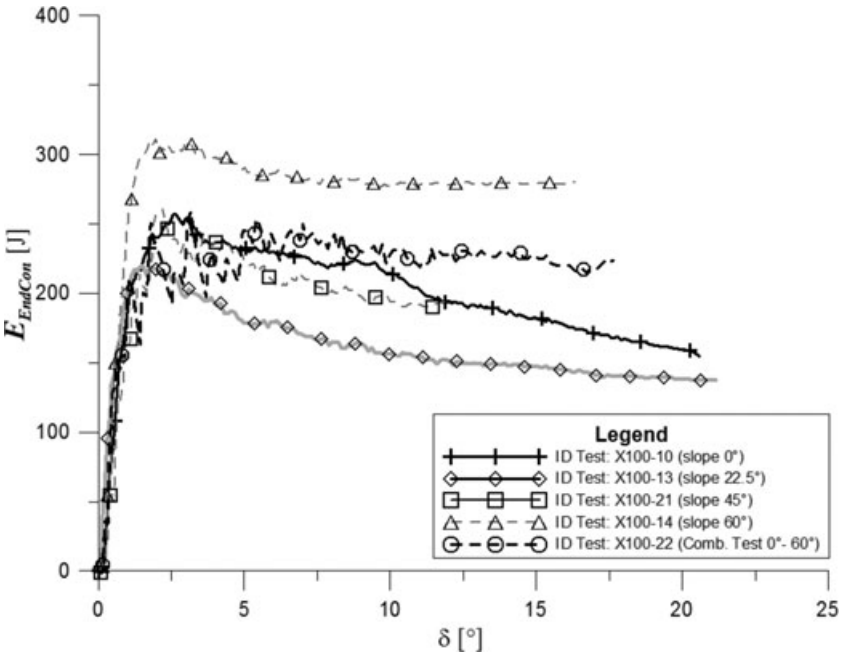

Fig. 16 Energy dissipated within the connection between the specimen and extensions.

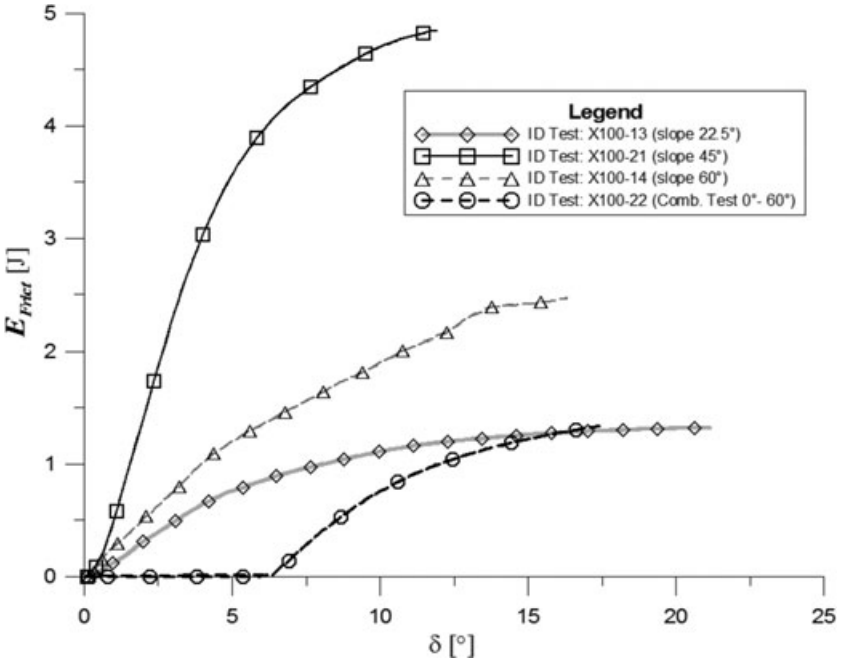

Fig. 17 Resulting friction energy loss acting in the system.

of two contributions

$$\overline{AF} = \cos(\vartheta) \cdot \frac{L_C/2 - a}{\cos(\vartheta + \gamma)}$$
$$\overline{FD} = \cos(\vartheta) \cdot \frac{L_C/2 + a}{\cos(\vartheta - \gamma)}. \tag{31}$$

We can now enforce the equivalence with the total length of the assembled specimen-extensions with the aim to extrapolate a as a function of γ and

$$a = \frac{\left[\frac{1}{\cos\vartheta} - \frac{1}{2} \cdot \left(\frac{1}{\cos(\vartheta + \gamma)} + \frac{1}{\cos(\vartheta - \gamma)}\right)\right]}{\left(\frac{1}{\cos(\vartheta - \gamma)} - \frac{1}{\cos(\vartheta + \gamma)}\right)} \cdot L_C \tag{32}$$

This quantity slightly changes if one also considers the axial stiffness of the specimen-extensions.

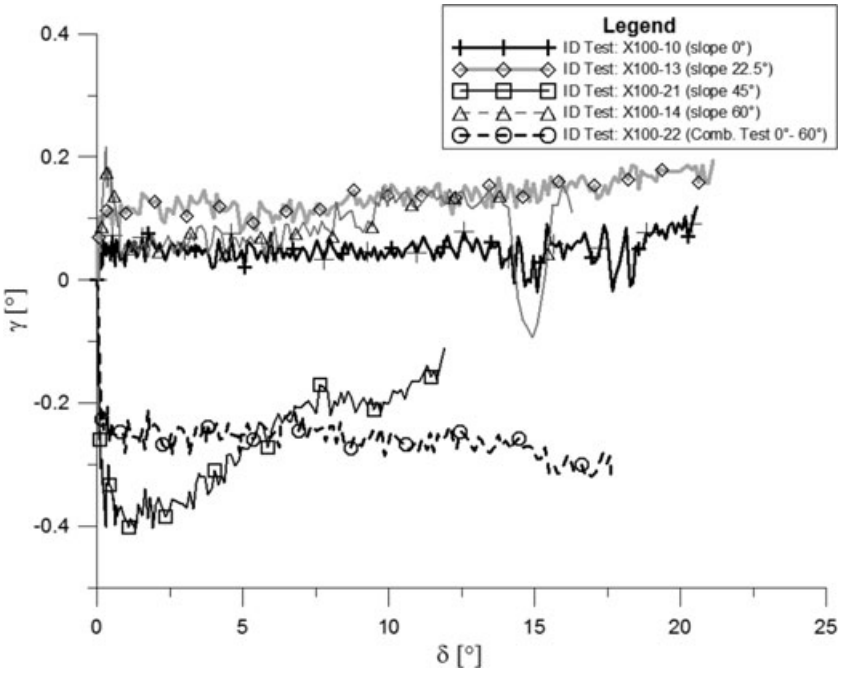

Fig. 18 Attitude of rectilinear bar for some slopes of the inclined supports.

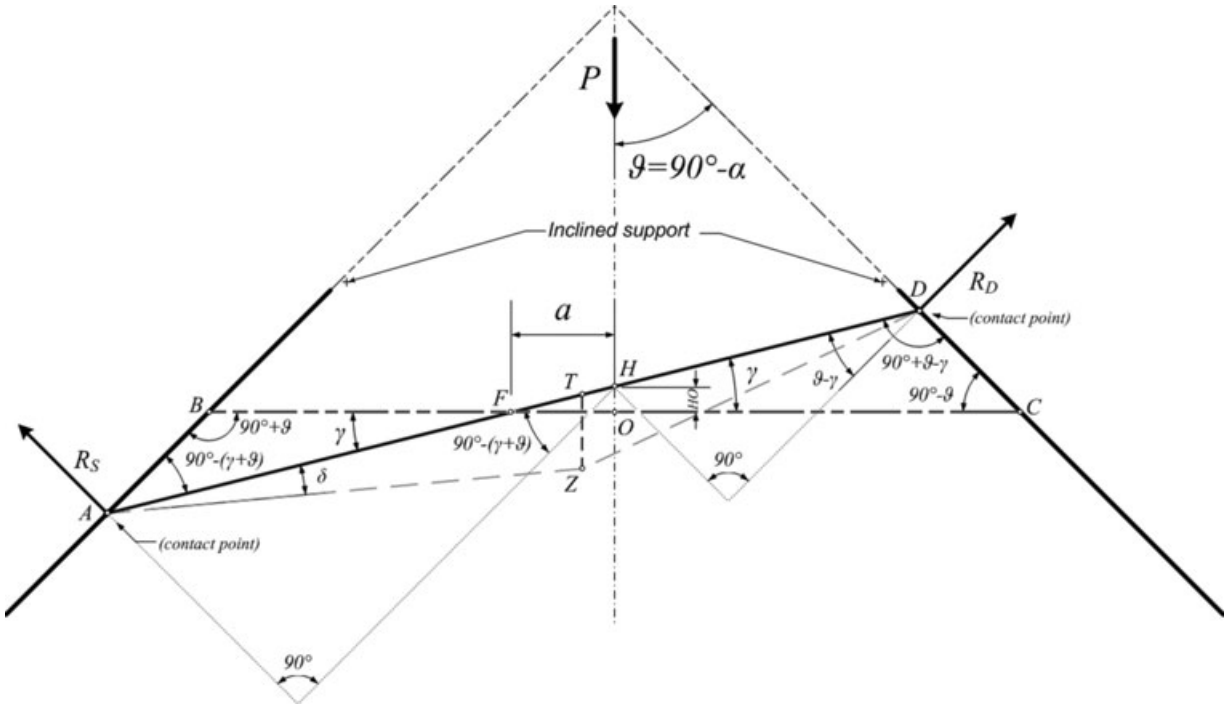

Fig. 19 Geometrical representation of the specimen (dashed-dot-dot: symmetric; blue: generci attitude).

$$a' = a\frac{L_C + \frac{P}{k}\cdot\tan(\vartheta)}{L_C} \tag{33}$$

If the system moves on a side of an amount a', the point where the hammer contacts the specimens lifts up of a quantity:

$$\overline{OH} = a'\cdot\tan(\gamma) \tag{34}$$

Furthermore, the specimen rotates around point O of a quantity δ as a consequence of its bending and its compliance change due to fracture advance. Considering all together these effects, the point where the load is applied drops

$$Drop = a'\cdot\tan(\gamma) - \frac{L_C}{2}\tan(\delta)\,. \tag{35}$$

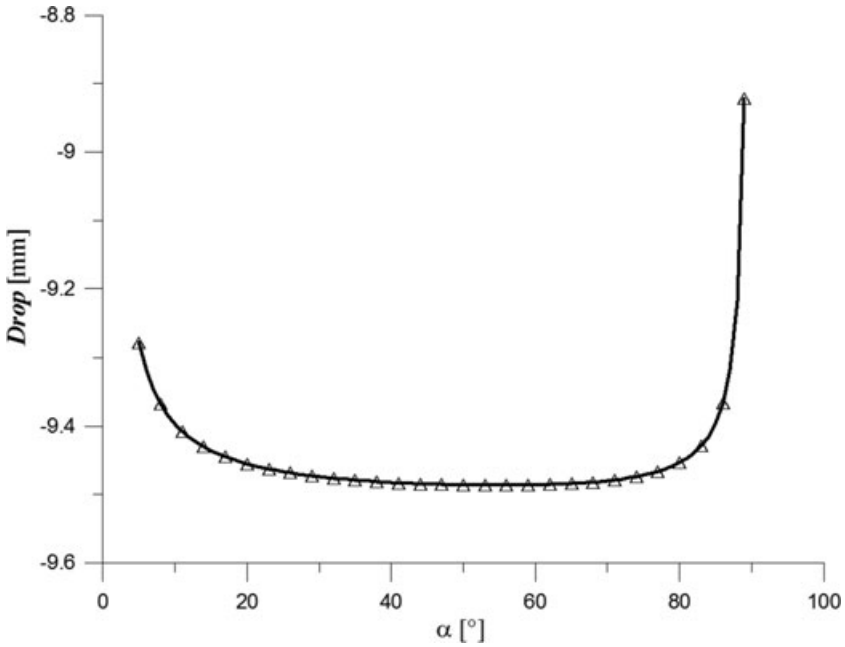

Fig. 20 Value of the *Drop* versus the angle of the inclined supports.

This last expression contains a small approximation since $\overline{OH}$ is considered very close to $\overline{TZ}$when δ and γ are small compared to.

Using point H as the pole for momentum equilibrium of the normal reaction loads at the supports, one can find a residual moment that should be supplied to reach γ

$$M_{Res} = \frac{P}{\tan(\vartheta)} \cdot \left\{ \left[\overline{AF} + a'/\cos(\gamma) \right] \cdot \sin(\vartheta + \gamma) - \left[\overline{FD} - a'/\cos(\gamma) \right] \cdot \sin(\vartheta - \gamma) \right\} \quad (36)$$

This moment unbalance can be thought as supplied by a horizontal load given by the hammer; its value being:

$$\mathrm{F_{Res}} = \frac{2 \cdot \mathrm{M}_{res}}{H} \quad (37)$$

In Fig. 20 the values of *Drop*, when increasing the support slopes, are shown. When the *Drop* increases there is an additional amount of energy made available for the misalignment γ. This is to say that the intermediate values of α correspond to the tendency to have a higher trend towards misalignment. Furthermore, from Fig. 21, showing the horizontal force that should be supplied to reach the

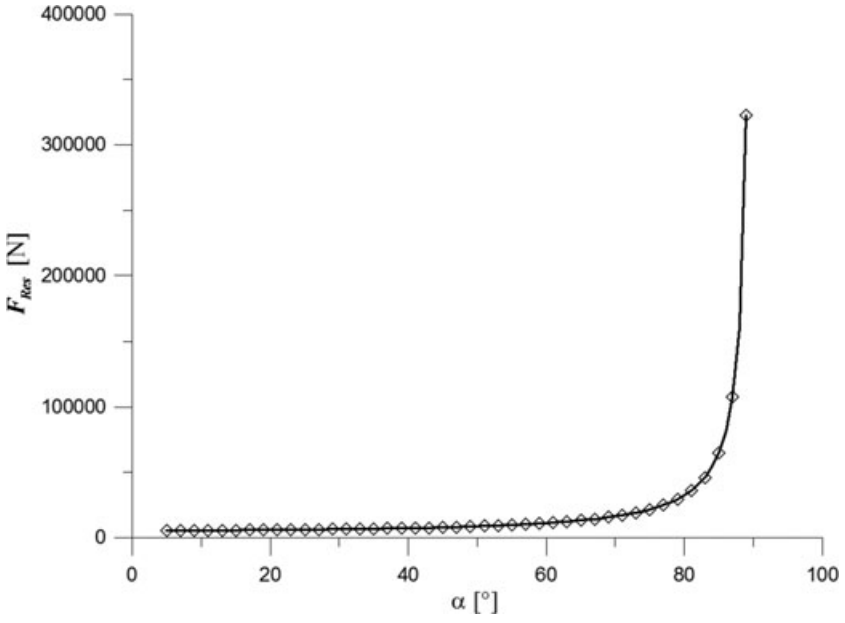

Fig. 21 Residual load versus the angle of the inclined supports.

misalignment, we see that this contribution is stable for a while, then it increases significantly. The two aspects together indicate that the perfectly horizontal configuration is always stable; but the maximum tendency towards misalignment is reached when the support slopes approach 45–50°, as it results from experiments.

However, for the next tests that will take advantage of still higher support slopes, it is advisable to reduce the radius of the hinges applied to the extensions to gain stability. The use of lower radius pins modifies the whole kinematics of the system. The results is a behavior very close to the one represented in Fig. 19, if one considers a higher value associated to the length of $\overline{BC}$, due to the increasing distance between the two contact points. Fig. 22 shows graphically the previous statement.

A final important check concerns the magnitudes of the stretching energies that are produced during the tests. These values result to be negligible if compared to the energy put in the system, as shown in Fig. 23. One can however observe that, even if the energies are small, the values increase according to slopes. This amount should be carefully taken into account for, when higher support slopes will be considered, in the next time.

CONCLUSIONS

The paper deals with a study intended to modify the DWT Tests performed on full thickness specimens taken from pipelines. The objective is to arrange the test so that the stress field in the region, where the crack

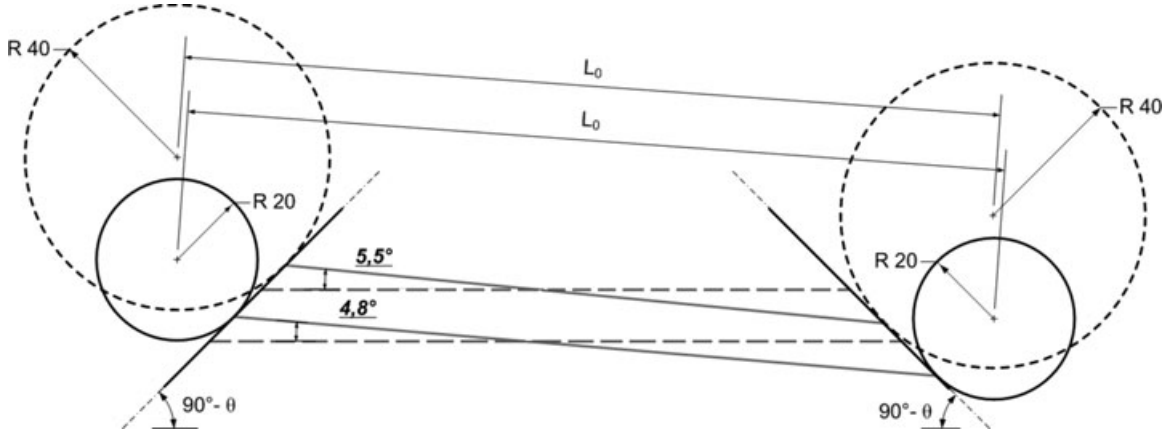

Fig. 22 Change of the specimen disposal for two hinge radius.

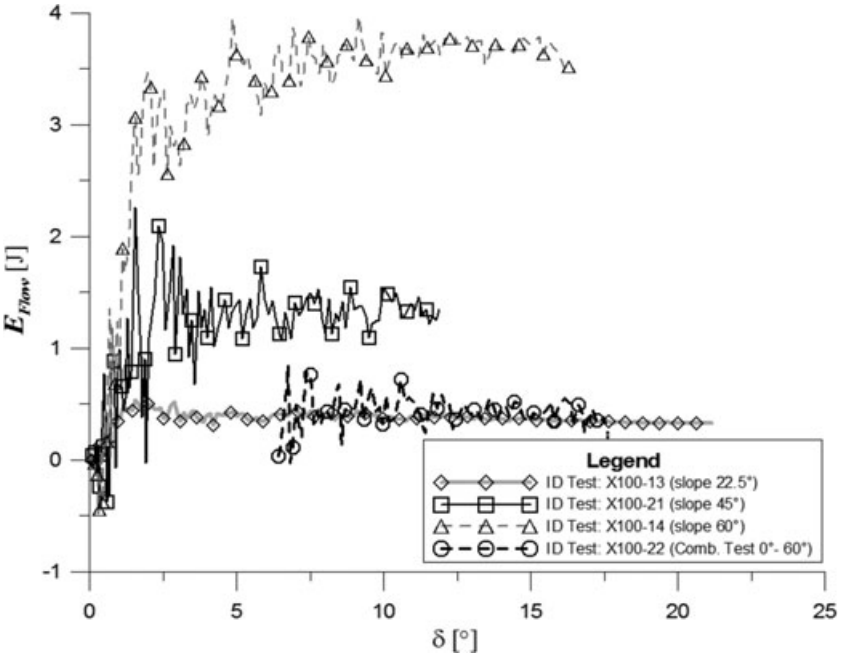

Fig. 23 Stretching energy of the specimen caused by the inclined supports.

develops, maintains its value as it occurs on pipelines. From this point of view, it is shown that the slope angle of the supports must reach values as high as 75° to induce a persistent stress that is comparable with the hoop stress, experienced by the pipe, when a longitudinal crack propagates.

The method takes advantage of image identification and processing of some markers applied on the system components; thus, the frame sequence allows to monitorize the fracture mechanism.

Standard DWT specimens have been used; this was made possible through the application of two extensions on the specimen itself. The adoption of the extensions allows to reduce the compression plasticity under the hammer, which generally affects the significance of the results. However, the extensions could be eliminated if non-standard specimens (longer) are extracted and flattened from the pipe.

The advantages of this new set-up are widely discussed in the paper, where the analytical derivation of all quantities presented is shown. The final objective is a tool able to compute several parameters such as nominal stresses, loads, energies and kinematical variables.

The tests were accurately discussed on a X100 steel, but the same tool applied on X60 steel confirmed the accuracy of the measurement set-up.

When introducing inclined sliding planes, it is advisable to represents the DWT Test results in terms of bending moment – relative rotation instead of simple load – displacement. By this point of view, all data originating by different support slopes can be joined together.

In this paper the method is applied on quasi-static tests; dynamic DWTT of course behaves differently. Here, the interest is pointed out on the overall method and the check of it instead than on experimental results: all the equilibriums and energy balances are well satisfied.

The same strategy could be applied to dynamic tests thus performing DWTT under crack propagation conditions that result closer to pipeline fracture propagation. In a simpler way, the deep static analysis conducted in this paper could open the way to modify the standard instrumented DWT Tests by the adoption of inclined supports, even excluding the image-processing procedure.

Acknowledgements

The authors acknowledge the *Centro Sviluppo Materiali S.p.A.* for the support given to this research.

REFERENCES

1 Rothwell, A. B. (2000) Fracture propagation control for gas pipelines – past, present and future. In: *Pipeline Technology* (Edited by R. Denys). Vol. 1, 387–405. Gulf Professional Publishing, Brugge-Belgium.

2 Takeuchi, I., Makino, H., Okaguchi, S., Takahashi, N. and Yamamoto, A. (2006) Crack arrestability of high-pressure gas pipelines by X100 or X120. In: *Proceedings of the 23rd World Gas Conference*, Amsterdam.

3 Andrews, R. M. and Batte, A. D. (2003) Developments in fracture control technology for gas pipelines utilising high strength steels. In: *Proceedings of the 22th World Gas Conference*, Tokyo, Japan; 1–5.

4 Fonzo, A., Salvini, P., Mannucci, G. and Di Biagio, M. (2002) Full history burst test through finite element analysis. In: *Proceedings of IPC2002: The International Pipeline Conference*, Calgary, Canada.

5 Maxey, W. A. (1974) Fracture initiation, propagation and arrest. In: *Proceedings of the 5th Symposium on Line Pipe Research, American Gas Association. Catalogue Number L30175 paper J-1*, Arlington, VA.

6 Rothwell, A. B. (1997) Fracture propagation control measures for gas pipelines – Methane. In: *Proceedings of International Seminar on Fracture Control in Gas Pipelines*, Sydney.

7 Priest, A. H. and Holmes, B. (1983) Prediction of linepipe fracture behaviour from laboratory tests. *Int. J. Pressure Vessels Piping* **12,** 1–27.

8 O'Donoghue, P. E., Kanninen, M. F., Leung, C. P., Demofonti, G. and Venzi, S. (1997) The development and validation of a dynamic fracture propagation model for gas transmission pipelines. *Int J Pressure Vessels Piping* **70,** 11–25.

9 Mannucci, G., Di Biagio, M., Demofonti, G., Fonzo, A., Salvini, P. and Edwards, A. (2004) Crack Arrestor design by finite element analysis for X100 gas transportation pipeline. In: *Proceedings of the 4th International Conference on Pipeline Technology*, Ostend, Belgium; 9–13 May.

10 Berardo, G., Salvini, P. and Di Biagio, M. (2000) The Application of cohesive model to dynamic ductile fracture tests. In: *Proceedings of the 13th European Conference on Fracture*, San Sebastian, Spain.

11 Fonzo, A, Salvini, P, Mannucci, G, Demofonti, G, Di Biagio, M and Edwards, A. (2005) A finite element model to simulate crack arrestor constraint effect on gas-pipeline. In: *Proceedings of the 11th International Conference on Fracture*, Torino.

12 Schwalbe, K. H., Newman Jr J. C. and Shannon, Jr J. L. (2005) Fracture mechanics testing on specimens with low constraint–standardisation activities within ISO and ASTM. Eng. *Fract. Mech.* **72,** 557–576.

13 Priest, A. and Holmes, B. (1981) A multi-test piece approach to the fracture characterization of linepipe steels. *Int. J. Fract.* **17,** 277–299.

14 Shterenlikht, A., Hashemi, S. H., Howard, I. C., Yates, J. R. and Andrews, R. M. (2004) A specimen for studying the resistance to ductile crack propagation in pipes. *Eng. Fract. Mech.* **71,** 1997–2013.

15 Darcis, P. P., McCowan, C. N., Windhoff, H., McColskey, J. D. and Siewert, T. A. (2007) A specimen for studying the resistance to ductile crack propagation in pipes. *Eng. Fract. Mech.* **75,** 2453–2468.

16 Minotti, M. and Salvini, P. (2011) Deep fracture profile effect on DWT Test for pipeline characterization. In: *Proceedings of the Pipeline Technology Conference*, Hannover.

17 Di Biagio, M., Fonzo, A. and Salvini, P. (2004) Fracture propagation in DWT back slotted specimens. *Int. J. Fract.* **128,** 159–169.

18 Xu, S., Bouchard, R. and Tyson, W. R. (2007) Simplified single-specimen method for evaluating CTOA. *Eng. Fract. Mech.* **74,** 2459–2464.
19 Martinelli, A. and Venzi, S. (2001) Dependence of J tearing modulus, CTOA, and total fracture energy on specimen dimension. *Eng. Fract. Mech.* **68,** 1575–1590.
20 Newman, J. C., James, M. A. and Zerbst, U. (2003) A review of the CTOD/CTOA fracture criterion. *Eng. Fract. Mech.* **70,** 371–385.
21 Marotta, E., Minotti, M. and Salvini, P. (2011) Effect of fracture tunneling in DWT Tests. *Eng. Fract. Mech.* Vol. 81, pp. 33–42, February 2012.
22 Salvini, P., Berardo, G., Demofonti, G. and Mannucci, G. (1999) A fracture process zone model for CTOA analysis. In: *Proceedings of the International Conference On Fracture Damage Mechanics*, Queen Mary & West field College University of London–London (UK); July 1999.
23 Martinelli, A. and Venzi, S. (1996) Tearing modulus, J-integral, CTOA and crack profile shape obtained from the load-displacement curve only. *Eng. Fract. Mech.* **53,** 263–277.
24 Berardo, G., Salvini, P., Mannucci, G. and Demofonti, G. (2000) On longitudinal propagation of a ductile fracture in a gas line pipe: numerical and experimental analysis. In: *Proceedings of the International Pipeline Conference IPC2000*, Calgary.
25 Fontana, A., Minotti, M. and Salvini, P. (2010) Cohesive Release Loads in a General Finite Element Model of a Propagating Crack. *J. Key Eng. Mater.* ***417–418,*** 517–520.